AN IMPROVED PANEL METHOD FOR UNSTEADY AEROFOIL FLOWS

N. Vlachos[1] and S.P. Fiddes[2],
Department of Aerospace Engineering, University of Bristol
Bristol, UK

Abstract

This paper presents some improvements to a low-order panel method for computing unsteady, inviscid, incompressible potential flows. An explicit Kutta condition for equalization of the trailing edge pressures is defined and implemented iteratively in a linearised form yielding improved prediction of pressures at the trailing edge. The wake shedding model, which possesses an arbitrary parameter for this type of low-order method, is also examined and a method for removing the indeterminacy of the wake-shedding parameter on a rational basis is put forward. These improvements are incorporated into a two-dimensional panel method and results obtained for a NACA0012 section in transient and oscillatory motions. Results are compared with those from a moving-mesh finite-volume Euler solver for incompressible flow, and the two methods are shown to agree closely for the lift and pitching moment predictions, while comparison of the computed wakes shows major differences. Additional results are also shown for the panel method for the case of the convection of a point vortex past a moving aerofoil and its wake.

Nomenclature

Symbols

c	aerofoil chord (solution characteristic length)
C_L	section lift coefficient
C_M	section pitching moment coefficient (about $x/c = 0.25$)
N, N_W	number of panels around the aerofoil section and number of wake panels
n_{pc}	solution time-steps per cycle of motion
p	pressure
q	surface-tangent perturbation velocity
$\mathbf{r}_o$	intrinsic position vector (x', y') from center of rotation
$\mathbf{r}$	vector from singularity to point of influence
$\hat{\mathbf{s}}, \hat{\mathbf{n}}$	surface-panel tangent and normal vectors
S_B, S_W	body and wake surfaces
u, v	flow velocity components in (x, y)
$\mathbf{V}_o$	inertial velocity of intrinsic frame origin
x, y	inertial frame coordinates
t, τ	time and non-dimensional time $\tau = tU/c$
α	aerodynamic incidence
Γ	circulation
γ	vorticity
$\Delta C_{p_{TE}}$	pressure coefficient difference between upper and lower surfaces at the
δs	panel chord-length trailing edge
ζ_w	wake shedding parameter
μ	surface doublicity strength (equivalent to $\phi - \phi_i$)
ϕ	perturbation velocity potential
σ	surface source density (equivalent to $\frac{\partial \phi_i}{\partial n} - \frac{\partial \phi}{\partial n}$)
Ω_o	rate of rotation of intrinsic frame
ω	angular frequency

Superscripts/Subscripts

$'$	intrinsic (body-fixed) frame quantity
$\tilde{}$	previous time level quantity
$\bar{}$	quantity normalised against steady-state value
$_i$	quantities internal to S_B or body panel index
$_{U,L}$	upper and lower surface at the trailing edge
$_{B,W}$	body and wake quantities respectively
$_{ss}$	steady-state

[1] graduate student
[2] Professor

Introduction

In many panel methods, the Kutta condition of classical aerofoil theory has been applied in a manner that *implicitly* accounts for the physical effects of viscosity at points of high surface curvature, simultaneously fixing the level of bound circulation of lifting surfaces. In its analytic application for steady flow about two-dimensional aerofoils, the Kutta condition

specifies that the flow separates from the aerofoil surface at the aerofoil trailing edge such that the flow speeds on both surfaces of the trailing edge remain finite[1]. From this follow restrictions on the flow velocity at the edge different for finite-angle and cusped trailing edge geometries [6], both cases having in common equal pressures on upper and lower surfaces at the trailing edge.

This equalization of pressure on either side of a trailing edge is also used to define the Kutta condition in unsteady aerofoil problems where the conditions on the velocity at the trailing edge are then modified by the sense of vorticity being shed from the edge[4, 6]. It has been suggested that there is an upper limit to the frequency range for which this interpretation of the Kutta condition can be applied [10, 11, 12, 13, 14], but such extreme conditions will not be considered in this work.

A simple 'implicit' Kutta condition, is used in some well known low-order panel methods for steady and unsteady flows [1, 7, 8, 15]. This paper will present an implementation of the 'equal-pressure' Kutta condition and treatment of the aerofoil trailing edge in the framework of a low-order panel method. This improved form of the Kutta condition is needed for unsteady flow to improve the prediction of surface pressure especially in the vicinity of trailing edge. The goal of this work is an implementation of this condition that does not require higher order singularities or geometry representation on any part of the solid or wake surfaces modelled and must not incur heavy computational costs. Furthermore, it is necessary to tackle the problem of the free wake-shedding parameter which is a feature of this type of low-order panel method [1, 5].

Low-order panel methods are very versatile, and developments of the approach described here can ultimately be applied to the solution of unsteady incompressible potential flows about multiple three-dimensional deforming geometries. For simulations of such complexity, simplicity and computational efficiency are paramount and are the primary incentives for pursuing improvements for this panel method.

Solution Method

Doublet and source singularities are used to represent the surface of two-dimensional profiles in incompressible potential flow where the governing equation (for continuity) is Laplace's equation

$$\nabla^2\phi = 0 \tag{1}$$

and the potential ϕ is related to the flow velocity by

$$\nabla\phi = (u, v) \tag{2}$$

Since Eq. (1) is a linear differential equation the principle of superposition applies and the complete solution can be assembled from a combination of elementary solutions. The elementary solutions used here include the two-dimensional vortex, doublet and source singularities which satisfy Laplace's equation in the region of the flow around them[1]. Uniform distributions of sources and doublets on flat panels are used for the body, while the wake is represented by doublet panels only (equivalent to point vortices at the doublet panel junctions.)

The total potential at a point in the flow is the summation the global ϕ influence of all the σ and μ singularities distributed over S_B and S_W

$$\phi(x,y,z) = \frac{1}{4\pi}\int_{S_{B,W}} \mu \frac{\partial}{\partial n}\left(\frac{1}{\mathbf{r}}\right) ds - \frac{1}{4\pi}\int_{S_B} \sigma\left(\frac{1}{r}\right) ds \tag{3}$$

The surfaces S_B and S_W are modelled by N and N_W discrete panels respectively, so the discrete form of Eq. (3) is needed

$$\phi_i(x,y) = \sum_{j=1}^{N} \mu_j A_{i,j} + \sum_{j=1}^{N} \sigma_j B_{i,j} + \sum_{k=1}^{N_W} \mu_k C_{i,k} \tag{4}$$

The influence coefficients $A_{i,j}$, $B_{i,j}$ and $C_{k,j}$ which replace the integrals in Eq. (3) for constant unit strength doublet and source panels are given by

$$A_{i,j} = \frac{1}{4\pi}\int_{S_i} \frac{\partial}{\partial n}\left(\frac{1}{\mathbf{r}_{i,j}}\right) ds \tag{5}$$

$$B_{i,j} = -\frac{1}{4\pi}\int_{S_i} \frac{1}{r_{i,j}} ds \tag{6}$$

$$C_{i,k} = \frac{1}{4\pi}\int_{S_k} \frac{\partial}{\partial n}\left(\frac{1}{\mathbf{r}_{i,k}}\right) ds \tag{7}$$

where the integrals are taken over the each of the body and wake panels denoted by S_i and S_k.

The solution aims to find the distributions of σ and μ that produce a flow-field which satisfies the physically correct boundary condition, i.e. zero flow through S_B. In the numerical solution, this is strictly true only at the discrete points where the boundary condition is enforced, in this case points just inside S_B at panel centres (the collocation points.)

The boundary condition is tackled in two steps in this method. Firstly, to nullify the local onset flow due to the kinematic velocity normal to S_B at each collocation point, σ set so that

$$\sigma = -(\mathbf{V}_o + \Omega \times \mathbf{r}_o) \cdot \hat{\mathbf{n}} \tag{8}$$

at each panel. This only satisfies the boundary condition *locally* and the σ distribution induces a perturbation potential to the *global* flow which does not yet

satisfy the tangency condition on S_B. Therefore, in the second step, the μ distribution must be adjusted to nullify the *global* perturbation due to σ. Since the above also means that

$$\frac{\partial \phi_i}{\partial n} = 0 \tag{9}$$

and there are no singularities internal to S_B the Dirichlet boundary condition can be enforced[1]

$$\phi_i = 0 \tag{10}$$

where ϕ_i is given by Eq. (4). This results in the following matrix equation for finding the needed combination of surface doublet strengths (including a wake doublet panel)

$$\begin{bmatrix} A_{1,1} & A_{1,2} & \cdots & A_{1,N} & C_{1,W} \\ A_{2,1} & A_{2,2} & \cdots & A_{2,N} & C_{2,W} \\ \vdots & \vdots & \ddots & \vdots & \vdots \\ A_{N,1} & A_{N,2} & \cdots & A_{N,N} & C_{N,W} \end{bmatrix} \begin{bmatrix} \mu_1 \\ \mu_2 \\ \vdots \\ \mu_N \\ \mu_W \end{bmatrix} = \begin{bmatrix} \mathrm{RHS}_1 \\ \mathrm{RHS}_2 \\ \vdots \\ \mathrm{RHS}_N \end{bmatrix} \tag{11}$$

where

$$\mathrm{RHS}_i = \sum_{j=1}^{N} \sigma_j B_{i,j} + \sum_{k=1}^{W-1} \mu_k C_{i,k} \tag{12}$$

The above matrix equation has one more unknown than equations and requires an additional equation for a unique solution provided by applying a trailing edge condition.

Unsteady solution

The unsteady solution proceeds by time-stepping through a series of instantaneous solutions of Eq. (11) and a trailing edge condition. The solution is aware of the flow history through the strengths and positions of the wake singularities.

Changes in the level of aerofoil bound circulation result in the shedding of vorticity at the trailing edge, the strength of which is determined with the application of the Kutta condition. The is wake shed at points where the Kutta condition is enforced, one new free vortex being created for each solution time-step representing the vorticity shed during that time interval. The wake points are, in the time-steps subsequent to their creation, convected with the local flow velocity, the new positions being calculated by a simple Euler integration scheme which assumes a constant velocity history of each point during each time step. This scheme is known to exhibit cumulative error (worsened with large time-step size) and instability with small time-step size[16]. However, this scheme is considered adequate for the current computations. To limit the instabilities arising from close vortex spacing, a solid-body rotation vortex core of radius typically 10^{-5} of the aerofoil chord is applied in the calculation of velocity influence between free vortices.

The condition of zero net circulation production in the solution (the Kelvin condition) is automatically satisfied by this method since each wake doublet panel created is equivalent to two equal and opposite point vortices at the panel ends which together contribute zero net circulation.

Unsteady pressure

The form of the Bernoulli equation which relates the flow velocity and acceleration (in the inertial frame) to the pressure, in the absence of any force fields (e.g. neglecting gravity), is (from Ref. [1])

$$\frac{p}{\rho} + \frac{(\nabla \phi)^2}{2} + \frac{\partial \phi}{\partial t} = \frac{p_\infty}{\rho} \tag{13}$$

This defines the pressure in terms of the local flow conditions and the conditions at infinity where the flow perturbation is zero.

Since pressure on the surface of the body is of interest, the analysis is restricted to the external velocity potential and its derivatives on S_B. The $\phi(x, y)$ field used in Eq. (13) is an instantaneous sampling of the perturbation field induced by the singularities bound to and moving with S_B and S_W. In addition to the $\partial\phi/\partial t$ due to the fluctuation in singularity strengths, a point fixed in (x, y) will, in general, also perceive a change in ϕ with time due to the movement of the singularities. To obtain the total $\partial\phi/\partial t$ for a point fixed in inertial space the following transformation is needed

$$\left.\frac{\partial \phi}{\partial t}\right|_{x,y} = \left.\frac{\partial \phi}{\partial t}\right|_{s,n} + \left.\frac{\partial \phi}{\partial s}\right|_{n,t} \left.\frac{\partial s}{\partial t}\right|_{x,y} + \left.\frac{\partial \phi}{\partial n}\right|_{s,t} \left.\frac{\partial n}{\partial t}\right|_{x,y} \tag{14}$$

The potential carried by the body on the outside of S_B with doublicity μ is simply

$$\phi = \phi_i + \mu = \mu$$

from Eq. (10), which means that

$$\left.\frac{\partial \phi}{\partial t}\right|_{s,n} = \frac{\partial \mu}{\partial t} \tag{15}$$

As S_B moves through inertial space the component of flow velocity in the surface normal direction is

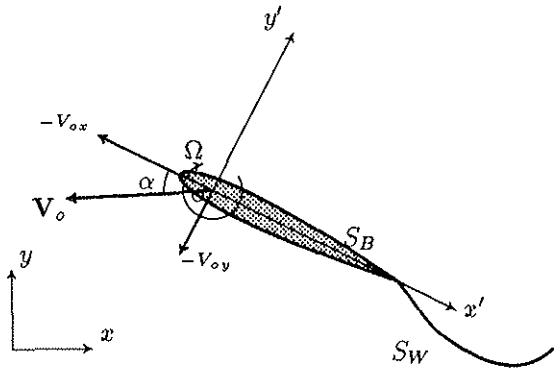

Figure 1: Inertial and aerofoil intrinsic coordinates

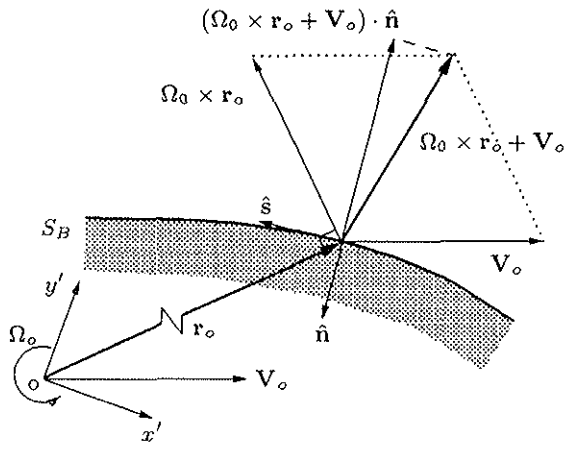

Figure 2: Detail of surface quantities

known directly from the local velocity of the surface since the surface will carry the fluid in the $\hat{\mathbf{n}}$ direction

$$\frac{\partial \phi}{\partial n} = (\mathbf{V}_o + \Omega_o \times \mathbf{r}_o) \cdot \hat{\mathbf{n}} = -\sigma \qquad (16)$$

In the $\hat{\mathbf{s}}$ direction the fluid moves relative to the (x, y) with the local tangential perturbation velocity (irrespective of $(\mathbf{V}_o + \Omega_o \times \mathbf{r}_o) \cdot \hat{\mathbf{s}}$) so in the $\hat{\mathbf{s}}$ direction we have

$$\nabla \phi \cdot \hat{\mathbf{s}} = \frac{\partial \phi}{\partial s} = \frac{\partial \mu}{\partial s} = q \qquad (17)$$

Combining the expressions of Eq. (16–17) and Eq. (15) yields the total inertial $\partial \phi / \partial t$

$$\left.\frac{\partial \phi}{\partial t}\right|_{x,y} = -\sigma \left.\frac{\partial n}{\partial t}\right|_{x,y} + q \left.\frac{\partial s}{\partial t}\right|_{x,y} + \left.\frac{\partial \mu}{\partial t}\right|_{s,n} \qquad (18)$$

where (s, n) are surface coordinates local to and fixed to each point on S_B and known in terms of (x', y'). Given the motion state of the body $(\mathbf{V}_o, \Omega_o)$ through (x, y), it can be shown that

$$\left.\frac{\partial s}{\partial t}\right|_{x,y} = -(\mathbf{V}_o + \Omega_o \times \hat{\mathbf{r}}_o) \cdot \hat{\mathbf{s}} \qquad (19)$$

$$\left.\frac{\partial n}{\partial t}\right|_{x,y} = -(\mathbf{V}_o + \Omega_o \times \mathbf{r}_o) \cdot \hat{\mathbf{n}} = \sigma \qquad (20)$$

The full expression relating the local surface conditions with far-field conditions now becomes (from Eq. 13)

$$\frac{p_\infty - p}{\rho} = \frac{1}{2}(q^2 - \sigma^2) + \frac{\partial \mu}{\partial t} - q(\mathbf{V}_o + \Omega_o \times \mathbf{r}_o) \cdot \hat{\mathbf{s}} \qquad (21)$$

To obtain an expression for C_p from the above, it is necessary to choose a velocity which defines a reference stagnation pressure. For the calculation of the force/moment coefficients to be possible via integration of the C_p around the section the reference velocity must be constant over S_B. The most usual choice is the translational velocity of the whole body through (x, y)

$$V_{ref} = |\mathbf{V}_o|$$

although other reference speeds must be chosen for cases of pure rotation.

Eq. (21) in terms of the reference flow speed now yields the expression for the pressure coefficient on the body surface

$$C_p = \frac{1}{V_{ref}^2}(\sigma^2 - q^2 + 2q(\mathbf{V}_o + \Omega_o \times \mathbf{r}_o) \cdot \hat{\mathbf{s}} - 2\frac{\partial \mu}{\partial t}) \qquad (22)$$

where

$$C_p = \frac{p - p_\infty}{\frac{1}{2}\rho V_{ref}^2} \qquad (23)$$

Unsteady Kutta Condition

The commonly used implicit form of the Kutta condition, implemented here for comparison, specifies for steady flow [1]

$$\gamma_U - \gamma_L = 0$$

In the case of this low order panel method, this condition is replaced with

$$\sum \Gamma_{TE} = 0$$

(see Fig. 3) and is implemented by

$$\mu_N + \mu_W - \mu_1 = 0 \qquad (24)$$

In conjunction with the Kutta-Joukowski theorem this equation implies that the loading at the trailing edge is zero. Hence, the pressures at the trailing edge should be equal and the implicit condition of Eq. (24) should affect the nearby μ solution such that this results. The solution has a direct effect on the trailing

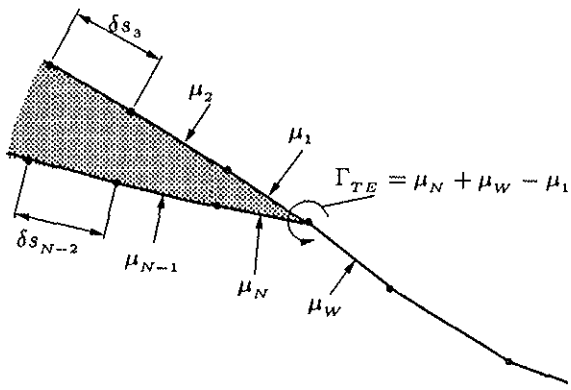

Figure 3: Detail of trailing edge panels

edge pressures through $\partial\mu/\partial s$. This is approximated by first order finite differencing of the step-wise continuous μ. However, it has been found that Eq. (24) does not provide sufficient control over the distribution of the discrete values of μ to result in equal trailing edge pressures as calculated in the post-processing.

In unsteady flow, the inadequacy of Eq. (24) is worsened by the omission of the $\partial\phi/\partial t$ component of the unsteady pressure. The condition which must now be applied, derived from Eq. (22) for $\Delta C_{P_{TE}} = 0$ at the trailing edge, is

$$q_U^2 - \sigma_U^2 + 2\left.\frac{\partial\mu}{\partial t}\right|_U - q_L^2 + \sigma_L^2 - 2\left.\frac{\partial\mu}{\partial t}\right|_L - 2q_U(\mathbf{V}_o + \Omega\times\mathbf{r}_o)\cdot\hat{\mathbf{s}}_U + 2q_L(\mathbf{V}_o + \Omega\times\mathbf{r}_o)\cdot\hat{\mathbf{s}}_L = 0 \quad (25)$$

This can not be implemented directly in the solution of the linear boundary condition equations since there are unknown quadratic terms of μ_i in the velocity q^2. In order to avoid the computational overhead of solving with a non-linear equation an approximation is needed which will linearise Eq. (25). The technique employed by this panel method, introduced by Bose[2], is to replace the quadratic perturbation velocity terms with products of the current (unknown) velocity q and the perturbation velocity at the previous time level $\tilde{q}$, i.e. to assume that

$$\left(\frac{\partial\mu}{\partial s}\right)^2 \approx \left(\frac{\partial\mu}{\partial s}\right)\left.\frac{\partial\mu}{\partial s}\right|_{t-\Delta t} = q\tilde{q} \quad (26)$$

The linearised trailing edge condition implemented is now

$$q_U\left(\tilde{q}_U - 2(\mathbf{V}_o + \Omega\times\mathbf{r}_o)\cdot\hat{\mathbf{s}}_U\right) - q_L\left(\tilde{q}_L - 2(\mathbf{V}_o + \Omega\times\mathbf{r}_o)\cdot\hat{\mathbf{s}}_L\right) - \sigma_U^2 + \sigma_L^2 + 2\left.\frac{\partial\mu}{\partial t}\right|_U - 2\left.\frac{\partial\mu}{\partial t}\right|_L = 0 \quad (27)$$

The unknown q terms are replaced by their numerical analogues (second order)

$$q_U = -\left(\frac{2}{\delta s_1 + \delta s_2} + \frac{2\delta s_1}{\delta s_2(\delta s_1 + \delta s_2)}\right)\mu_1 + \left(\frac{2}{\delta s_1 + \delta s_2} + \frac{2\delta s_1}{\delta s_2(\delta s_1 + \delta s_2)} + \frac{2\delta s_1}{\delta s_2(\delta s_2 + \delta s_3)}\right)\mu_2 - \left(\frac{2\delta s_1}{\delta s_2(\delta s_2 + \delta s_3)}\right)\mu_3 \quad (28)$$

$$q_L = \left(\frac{2}{\delta s_N + \delta s_{N-1}} + \frac{2\delta s_N}{\delta s_{N-1}(\delta s_N + \delta s_{N-1})}\right)\mu_N - \left(\frac{2}{\delta s_N + \delta s_{N-1}} + \frac{2\delta s_{N-1}}{\delta s_{N-1}(\delta s_N + \delta s_{N-1})} + \frac{2\delta s_N}{\delta s_{N-1}(\delta s_{N-1} + \delta s_{N-2})}\right)\mu_{N-1} + \left(\frac{2\delta s_N}{\delta s_{N-1}(\delta s_{N-1} + \delta s_{N-2})}\right)\mu_{N-2} \quad (29)$$

The application of the explicit trailing edge condition involves only unknown quantities (in this case, μ_i) on the aerofoil surface in an equation of the form

$$A_{N-2}\mu_{N-2} + A_{N-1}\mu_{N-1} + A_{N-2}\mu_N - A_3\mu_3 - A_2\mu_2 - A_1\mu_1 = RHS_{N+1} \quad (30)$$

Note that the strength of the shed wake panel μ_W is not directly coupled to the solution through Eq. (27) in this formulation. Instead is determined indirectly by its influence on the aerofoil boundary condition, i.e. through the coefficients $C_{i,W}$ in Eq. (11). This makes it possible to use any type of singularity to model the wake without affecting the implementation of the trailing edge condition, although it might then be necessary to explicitly enforce the Kelvin condition.

The approximation in Eq. (26) relies on the assumption that the perturbation velocities at the trailing edge do not change rapidly with time, and so Eq. (27) is less accurate with increasing rates of change and time-step size. In such cases, sub-iterations are performed within the same time level, the new values of q being used to update the approximation $\tilde{q}$, until the pressure difference is below some set tolerance, typically 0.005 of the reference dynamic head. The iterative process involves solving the matrix equation Eq. (11) changed only by the current set of coefficients from Eq. (30), and can be stopped once $\Delta C_{p_{TE}}$ is below some preset magnitude.

It has been found that this scheme works for most unsteady motions where the amplitudes and frequencies of the motions are not too great. The scheme is not convergent for all situations. At points in the solution where there are rapid accelerations at the trailing edge point, more iterations are required to attain the required difference in pressure, and in some cases the solution locks before the required pressure difference

is reached. It is sometimes useful to reset the coefficients of the iterative process with a sub-iteration using Eq. (24)), although after this the solution often locks in the same way. Doubling the precision of the computations gives only a slight improvement. Other more successful techniques for enhancing the sub-iteration process are being sought. One candidate which has not been sufficiently explored is adaptive time-stepping. Reducing the time step size will always make the approximation of Eq. (26) more accurate and convergence may be improved if the time-step size is reduced in proportion to rates of change of flow quantities at the trailing edge.

Wake Shedding Parameter

The current method does not provide the velocity exactly at the trailing edge or just off the trailing edge which would be needed to determine the position of each new shed wake vortex. Velocity calculation on or infinitesimally close to the trailing edge is as accurate as the interpolation/extrapolation scheme used to interpret the singularities in the vicinity. To bypass the lack of solution detail the average of the upper and lower surface trailing edge velocities is taken as the most representative of the time-average of the velocity with which the newest wake point is convected during the time-step it is generated. The wake doublet panel created does not constitute part of a streamline. It is assumed that the new vortex has followed a streakline to its current position (as computed by above approximation) but that the direction of the panel does not dictate the exact direction of flow off the trailing edge. Trying to prescribe or solve for such detail is inconsistent with the order of the current method

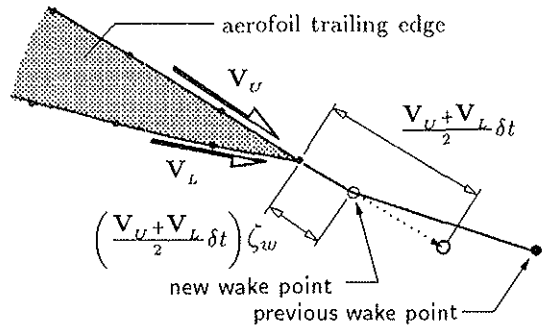

Figure 4: Detail of wake shedding at aerofoil trailing edge

The lack of detail in the wake shedding process introduces the parameter ζ_w to the method which is defined as the fraction of the local velocity-convected distance from the trailing edge at which the new wake point is placed. The same type of indeterminacy was encountered for the the PMARC code by Martin et al.[5]. In the latter case, the optimum value of ζ_w was sought by comparison with analytic results (Wagner and Theodorsen functions) for a thin flat plate in transient and oscillatory motions. Given that the latter are themselves approximations, this type of comparison is not entirely satisfactory as a calibration of ζ_w and another route is taken here.

More continuous representation of the shed vorticity may remove the ζ_w indeterminacy and it was attempted to replace the doublet panel at the trailing edge by a flat linear γ panel in order to verify the optimum ζ_w. This introduced an additional unknown $d\gamma/ds$ which it was hoped would allow the solution to determine automatically the center of vorticity within the new wake panel. The result was an oscillatory feedback instability and further work in this direction was abandoned. Another candidate approach was based on the work of Graham[17] using the complex-plane solution for the flow off an infinite wedge corner as a local solution at the trailing edge to determine the strength and positioning of the shed vorticity. This too was not taken to completion due to difficulty in interfacing the local solution with the global panel method solution and due to the prospect of poor extensibility to three dimensions. In general, it is not desirable to use higher order singularity distribution or geometry in the trailing edge region in order to preserve the simplicity of the method and to allow direct extension to a three-dimensional vortex lattice/panel method.

Fortunately, it becomes apparent that the method is, to a good extent, self-calibrating from the following observation: as $\Delta\tau$ is decreased the range of position that the new vortex point can take and the strength of the vortex both diminish. Therefore, as the time-step is decreased ζ_w becomes less significant. This seems consistent within the framework of the time discretisation since as $\Delta\tau \to 0$ a continuous vorticity sheet would result in making ζ_w practically ineffective in the limit (the shed vortex point would always coincide with the trailing edge). Obviously, due to numerical considerations (machine precision, vortex wake stability, memory, CPU time) this limit can not be approached to the extent that would fully calibrate the method, i.e. to the extent where ζ_w variation would have no effect at all on the results. However, calibration results can be obtained with small enough $\Delta\tau$ to give the desired maximum deviation in the results for a given change in ζ_w so that larger time-step runs can be used for longer simulations.

To show that ζ_w becomes less significant with decreasing $\Delta\tau$ a series of runs were performed with the NACA0012 aerofoil undergoing one cycle of $\alpha = 5^\circ \sin(2k\tau)$ pitch oscillation in steady forward flight. This was done for ζ_w values of 0.30 to 0.60 in equal increments of 0.10, repeating this series of calculations four times, initially with $\Delta\tau \approx 0.097$ and halving $\Delta\tau$ each time (see Fig. 6). The difference between the

solutions between successive values of ζ_w at the different $\Delta\tau$ clearly diminishes with decreasing $\Delta\tau$ showing that the effect of ζ_w becomes less significant. The solution C_M is used for the sensitivity analysis since it is most strongly affected by changes in ζ_w as seen in Fig. 5. In this case, which exhibits a maximum $C_M \approx 0.030$, reducing $\Delta\tau$ from 0.097 to approximately 0.012 reduces the maximum change in solution for $\Delta\zeta_w = 0.1$ from 10% to approximately 1% of maximum C_M. Assuming that the method converges to the correct solution with decreasing $\Delta\tau$ and that the discrete vortex shed must lie somewhere in the middle of the curve of continuous vorticity it is intended to represent, using any ζ_w in the range between 0.3 and 0.7 will yield a solution within a few percent of the datum solution, even for C_M which is sensitive to ζ_w variation.

The decreasing effect of ζ_w can only be exploited if for decreasing $\Delta\tau$ the method converges to one solution. The same set of runs used for the above analysis are used to show the convergence characteristics of the method. The C_M results of the smallest $\Delta\tau$ solution is used as a datum and the deviation of the other solutions from this is calculated within each ζ_w series. Different convergence characteristics are seen at different values of ζ_w. In all cases, as expected, the smaller $\Delta\tau$ runs show smaller deviation from the datum, although not with uniformity within the cycle (see Fig. 7). The inability of the iterative Kutta condition to converge at the ends of the cycle is believed to be the reason for this non-uniformity and, on the whole, the method tends to a single solution as $\Delta\tau \to 0$.

To find the optimum ζ_w for use with larger $\Delta\tau$ for each type of motion modelled a reference solution should be computed with $\Delta\tau \lessapprox 0.01$ and $\zeta_w \approx 0.5$. Then, results at the desired $\Delta\tau$ can be computed for a range of ζ_w values so that the optimum can be selected by comparison with the reference run which is known, from the above previous discussion, to produce results sufficiently independent of ζ_w. This calibration procedure would also be applicable to the three-dimensional extension of the current method. Alternatively, the calibration may be bypassed by obtaining the solutions with very fine time-step size and $\zeta_w \approx 0.5$.

Discussion of Results

Performance of the unsteady Kutta condition

Figure 9 compares the C_p error at the trailing edge with that of the linearised explicit Kutta condition of Eq. (27). The C_p error is plotted against the strength of the wake vortex shed during the time-step that the $\Delta C_{p_{TE}}$ was exhibited. This essentially plots the error in terms of a measure of the degree to which the flow is unsteady since the strength of the wake vortex being shed is inversely proportional to the rate of change of bound circulation (by the Kelvin theorem). Therefore, it is apparent that Eq. (24) produces error increasing in proportion to the degree to which the flow is unsteady and that the explicit Kutta condition of Eq. (27) performs significantly better.

Impulsive start at incidence

The transient response of the NACA0012 section started impulsively from rest into constant speed forward flight at $\alpha = 5°$ was computed. The results for some values of ζ_w are shown in Fig. 8. It is apparent that ζ_w has a stronger effect on the transient $\bar{C}_M$ response. The $\bar{C}_L$ response approaches Wagner's analytic indicial response for a flat plate [1] which predicts a starting $\bar{C}_L$ of 0.50. Perfect agreement is not expected since the panel method includes the effects of the time discretisation and of aerofoil thickness.

Oscillatory pitch motion

The NACA0012 section was used for a set of computations spanning a range of k from 0.02 to 0.30 shown in Fig. 5. The upper limit is considered low enough to avoid the regions of k where the validity of the unsteady Kutta condition is questionable. The NACA0012 section exhibits the collapse and reversal of the C_L loop at approximately $k = 0.2$ as predicted by Geissler[9] among others. The time-step is kept low in order to minimise ζ_w effects with $n_{pc} = 400$ used in the computations. Since $\Delta\tau$ is related to the number of time-steps used by $\Delta\tau = \pi/kn_{pc}$, it not constant for the runs at different frequencies. This is most noticeable for $k = 0.02$ from the magnified effect of ζ_w in the C_M response.

Wake convection sensitivity

In addition to recalculating the location of the wake as the aerofoil moves (solid-body translation and rotation), keeping the wake completely force-free requires the calculation of velocity influence (u and v components) at each of the current wake points from all other wake vortices and aerofoil singularities. This results in distortion of the wake and amounts to approximately $2N_W(N_B + N_W)$ velocity influence calculations per time-step. Each solution time-step a new wake-point is created so N_W is incremented and the computation is slowed nearly in proportion to N_W^2. Therefore it is desirable to reduce the portion of the wake for which the distorting components of flow velocity are applied, say for the K_{max} vortices nearest the trailing edge. Using the case of the NACA0012 section in $\pm 5°$ sinusoid pitching motion it is evident from Fig. 15 that the solution is relatively insensitive to the calculation of the distortion of the far wake. Reducing K_{max} results in significantly different wake

shapes (Fig. 16) but the effect on the solution is not noticed until $K_{max}/n_{pc} \approx 1\%$. Multiple body problems and simulations where the nature of the motion keeps the wake in proximity of the body may not be eligible for this computational saving.

Euler method comparison

The steady-flow aspects of the method can be verified by comparison with analytic results. However, for the unsteady aspects, such as the wake treatment, it is useful to compare with another method which solves for similar flow but which does not deal explicitly with the creation and convection of the shed vorticity. The method of Gaitonde[3] is used for comparison, as it solves the Euler equations (inviscid, incompressible but rotational flow) so fluid rotation is implicitly included. Unsteady solutions are obtained using artificial compressibility and a moving mesh on which a cell-centered finite volume scheme is implemented.

Initially, the resulting vortex wake from the two methods is compared to assess their ability to capture the flow history. The vorticity is extracted from the solutions of Gaitonde[3] for the $k = 0.30$ pitching motion case. This is done only at the solution instants corresponding to the quarter-phase positions of the pitching motion cycle for the NACA0012 section at the highest frequency compared ($k = 0.3$). The panel method wake points are superimposed on the resulting iso-γ contours in Fig. 14 with a graphical indication of the sign and strength of the panel method wake circulation.

The comparison indicates that the Euler solver is less capable of capturing and retaining the vorticity generated by the aerofoil, especially beyond five aerofoil chord lengths downstream. Decreasing grid density and increasing cell aspect ratio further from the aerofoil make it impossible for the Euler solver to resolve the wake as well as the panel method and it exhibits appreciable diffusion of the vorticity. Furthermore, since this is a deforming mesh method, the fluid behind the aerofoil is sampled by a grid which moves cyclicly through it as the trailing edge moves normal to the direction of the onset flow. This means that the wake is sampled successively by grid regions of varying density. Loss of flow detail because of this grid variation and the numerical dissipation incorporated in the method may be the main contributing factors to the diffusion and loss of vorticity.

The difference in wake-capturing capability does not seem to significantly affect the agreement for C_L and C_M seen in Fig. 12 where results are presented for the oscillatory pitch motion cases. The C_L agreement is excellent with both methods predicting the drop in hysteresis and the reversal of the C_L loop direction at $k = 0.20$. The agreement in C_M is good but deteriorates with decreasing frequency. This appears to be because the two methods predict slightly different steady-state solutions for $dC_M/d\alpha$ of the NACA0012 profile used. In order to gauge the agreement in a way which eliminates some of the effects of the post-processing (in this case, pressure integration around the profile), C_p distributions were also compared at the quarter-phase positions of the motion cycle. Fig. 13 shows the almost identical pressure distributions, the Euler solver capturing more detail of the C_p variation near the leading edge since over 90 points are used to sample the profile as opposed to the 60 panels used by the panel method.

Vortex interaction studies

The panel method was used to simulate the case of the NACA0012 profile at $\alpha = 0°$ flying past a free vortex. The interaction is simulated for the two cases (shown in Fig. 10 and Fig. 11) of a vortex of positive and negative circulation of the same magnitude starting five chord lengths in front and $0.10c$ below relative to the aerofoil centre. The oscillatory characteristics exhibited by the C_L and C_M results during the interactions indicate that the presence of the aerofoil wake damps the influence of the vortex and that modeling the wake is important in the correct prediction of the pressures during the interaction.

Conclusion

The linearised unsteady Kutta condition described here improves significantly the pressure prediction at the trailing edge for the simple transient and pitch-oscillation motions without excessive computational cost. However, improvement of the numerical implementation is needed in cases where the sub-iteration process fails to converge.

Comparison of panel method results using the new Kutta condition with the results of the cell-centered moving-mesh Euler solver of Gaitonde[3] shows good agreement between the two very different methods. This establishes the ability of the panel method to compute the unsteady incompressible flow about an aerofoil section with accuracy comparable to a finite volume method solving the Euler equations but in a fraction (typically 5%) of the computing time. Furthermore, the panel method, by 'fitting' the wake rather than capturing it (as the finite-volume method does), is capable of producing superior solutions for the wake shape. This superiority is more apparent at a distance from the trailing edge and is therefore more significant in multiple-body problems. It does not appear to be a factor in the current comparison which involves the computation of flow about a single aerofoil.

The wake convection process, which is one of the more computationally demanding aspects of the current method, is more significant for the wake points in the vicinity of the trailing edge and can be disabled for the wake beyond a certain distance (typically 5% of the motion cycle length) to reduce the computational effort, without noticeably affecting the solution on the aerofoil.

The effect of variations in the essentially 'free' wake-shedding parameter (ζ_w) which afflicts low-order methods of this type, can be controlled simply through reduction of the solution time-step size. It has been shown that decreasing $\Delta\tau$ nearly eliminates the effect of ζ_w (allowed to vary within a reasonable range) on the solution. This is true even for the aerofoil C_M which was shown to be especially sensitive to ζ_w. Therefore, selection of the optimum ζ_w for larger time-step calculations (for computational efficiency) can be selected by comparison (of a sample of the motion modelled) with a very fine time-step calibration solution.

With these improvements in the most critical areas of the Kutta condition and wake shedding treatment, the type of low-order singularity method described here promises to provide useful solutions for the unsteady potential flow about arbitrary three-dimensional geometries with relatively small computational cost. For unsteady flows in particular, the fact that the method only requires quantities on the body and wake surfaces makes it very attractive for more complex motions where surface deformations are involved.

References

[1] Katz, J. and Plotkin, A., *Low Speed Aerodynamics: From Wing Theory to Panel Methods*, McGraw-Hill, 1991.

[2] Bose, N., "Explicit Kutta Condition for an Unsteady Two-Dimensional Constant Potential Panel Method," *AIAA Journal*, Vol. 32, No. 5, May 1994, pp. 1078–1080.

[3] Gaitonde, A.L., "A Dual-Time Moving Mesh Method for 2D Unsteady Incompressible Flows Past Aerofoils," Bristol University, Aerospace Engineering Dept. Report No. 735, December 1995.

[4] Mangler, K.W. and Smith, J.H.B., "Behaviour of the Vortex Sheet at the Trailing Edge of a Lifting Wing," *Royal Aero. Soc. Journal*, Vol. 74, November 1970, pp. 906–908.

[5] Martin, and Kroo, "Comparison of PMARC and Analytic Results for Two-Dimensional Unsteady Airfoils," AIAA Paper 93-0636, 31st Aerospace Sciences Meeting and Exhibit, Reno, NV, Jan. 1993.

[6] Maskell, E.C., "On the Kutta-Joukowski Condition in Two-Dimensional Unsteady Flow," Royal Aircraft Establishment Tech. Memo. Aero 1451, Sept. 1972.

[7] Morino, L. and Kuo, C.C., "Subsonic Potential Aerodynamics for Complex Configurations: A General Theory," *AIAA Journal*, vol. 12, no. 2, pp. 191-197, 1974.

[8] Richason, T.F., Katz, J. and Ashby, D.L., "Unsteady Panel Method for Flows with Multiple Bodies Moving Along Various Paths," *AIAA Journal*, vol. 32, no. 1, pp. 62-68, Jan. 1994.

[9] Geissler, W., "Berechnung der Druckverteilung an oszillierenden Tragflächen mit endlicher Dicke in inkompressibler Strömung," DFVLR-AVA-Internal Rept. 76-48, 1976.

[10] Archibald, F.S. Unsteady Kutta Condition at High Values of the Reduced Frequency Parameter", *Journal of Aircraft*, vol. 12, pp. 545–550, 1975.

[11] Commerford, G.L. and Carta, F.O., "Unsteady Aerodynamic Response of a Two-Dimensional Airfoil at High Values of Reduced Frequency," *AIAA Journal*, vol. 12, no. 1, pp. 43–48, 1974.

[12] Satyanarayana, B., and Davis, S., "Experimental Studies of Unsteady Trailing Edge Conditions," *AIAA Journal*, vol. 16, no. 2, pp. 125–129, 1978.

[13] Fleeter, S., "Trailing Edge Condition for Unsteady Flows at High Reduced Frequency," AIAA Paper 79-0152, Jan. 1979.

[14] Poling, D.R., and Telionis, D.P., "The Response of Airfoils to Periodic Disturbances — The Unsteady Kutta Condition," *AIAA Journal*, vol. 24, no. 2, pp. 193–199, 1986.

[15] Katz, J., and Maskew, B., "Unsteady Low-Speed Aerodynamic Model for Complete Aircraft Configurations," *Journal of Aircraft*, vol. 25, no. 4, pp. 302–310, 1988.

[16] Moore, D.W., "A Numerical Study of the Roll-up of a Finite Vortex Sheet," *Journal of Fluid Mechanics*, vol. 63, pp. 225, 1974.

[17] Graham, J.M.R.,"Application of Discrete Vortex Methods to the Computation of Separated Flows", in Numerical Methods for Fluid Dynamics II, Oxford University Press, Oxford, pp. 273–302, 1986.

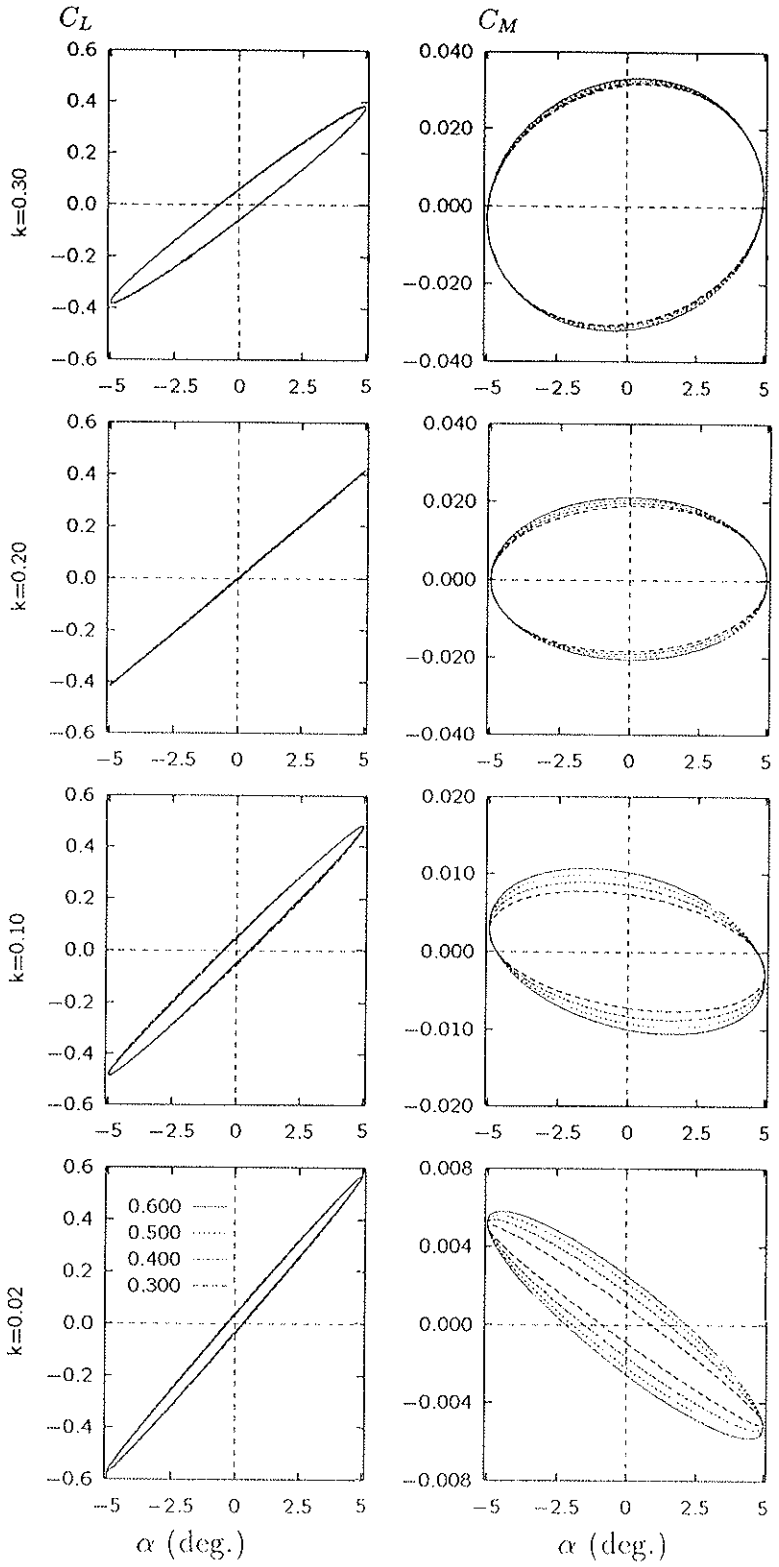

Figure 5: C_L and C_M of the NACA0012 section in $\alpha = \sin 2k\tau$ pitching motion at zero mean incidence for values of ζ_w from 0.300 to 0.600 ($N = 90$, $n_{pc} = 400$).

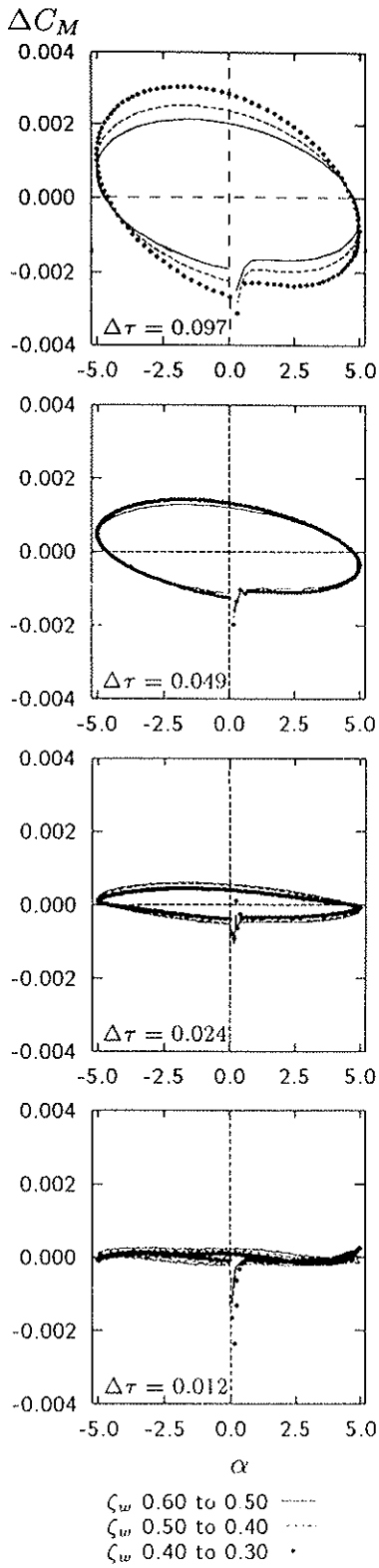

Figure 6: Effect of time-step size on C_M difference for increments in ζ_w of 0.10 (NACA0012 $\alpha = \sin 2k\tau$, $k = 0.300$).

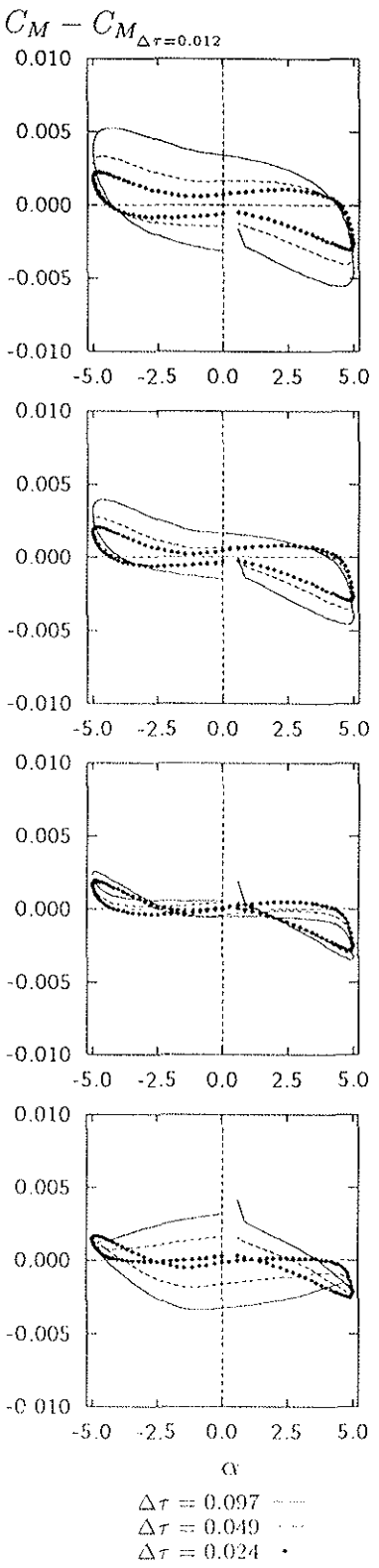

Figure 7: Effect of ζ_w on C_M convergence for decreasing time-step. The C_M solution for $\Delta\tau = 0.012$ is used as datum (NACA0012 $\alpha = \sin 2k\tau$, $k = 0.300$).

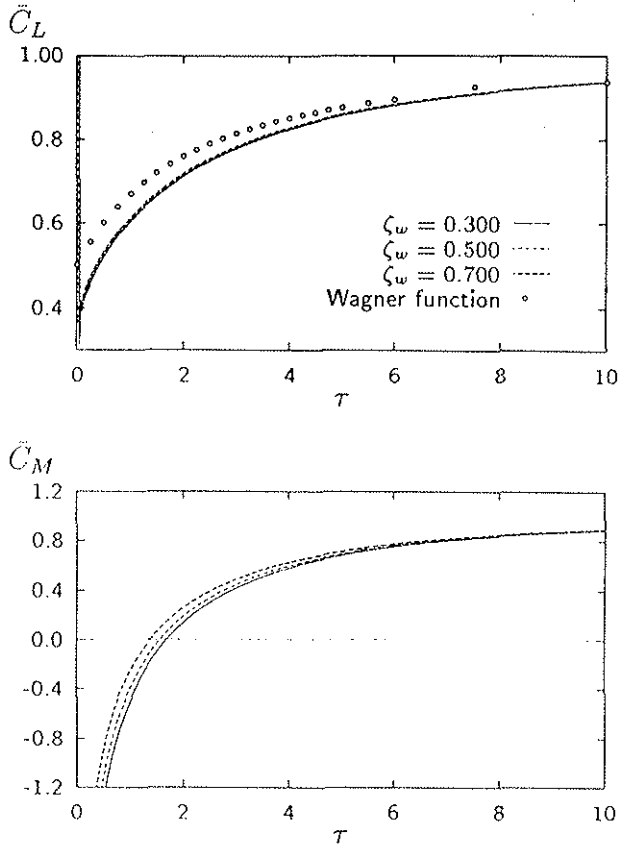

Figure 8: Transient C_L and C_M for NACA0012 section started impulsively into constant speed forward motion at $\alpha = 5°$. The normalising steady-state values are $C_{L_{ss}} = 0.585$ and $C_{M_{ss}} = 0.00532$ with $\Delta\tau = 0.02$.

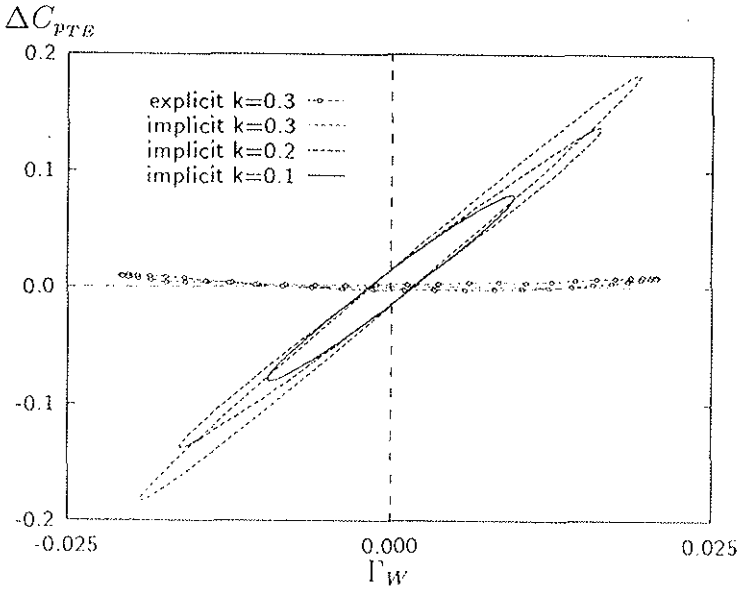

Figure 9: Performance of the Kutta conditions compared for the NACA0012 section in harmonic pitch motion ($\alpha = \sin 2k\tau$, $n_{pc} = 400$, ΔC_{pTE} tolerance for the explicit Kutta condition set to 0.005).

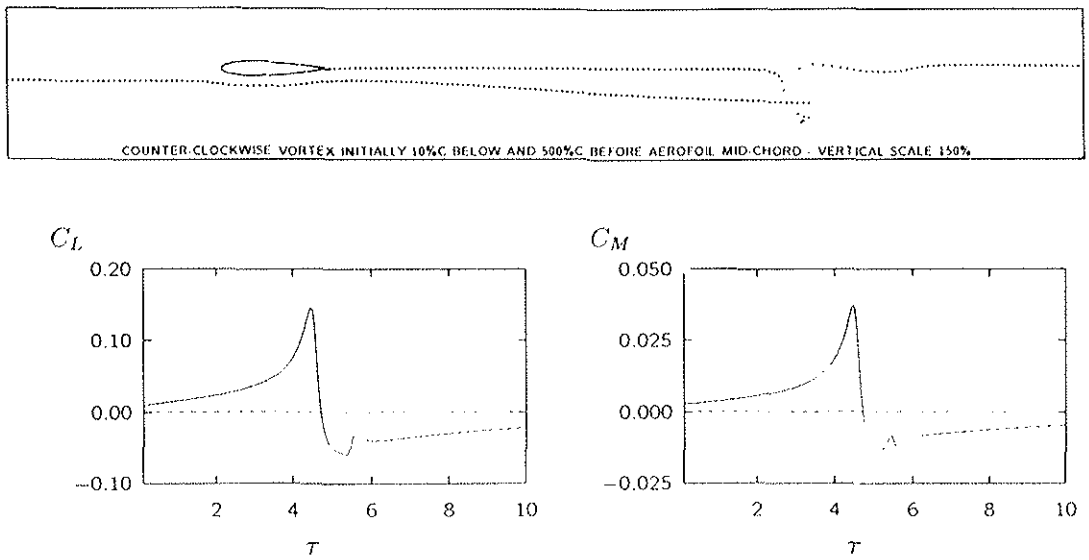

Figure 10: Vortex trajectory and C_L and C_M fluctuation during the interaction of a free vortex with a NACA0012 section flying at zero incidence relative to the undisturbed flow. The vortex passes the aerofoil leading edge at $\tau \approx 4.5$. ($\Gamma = -0.1$)

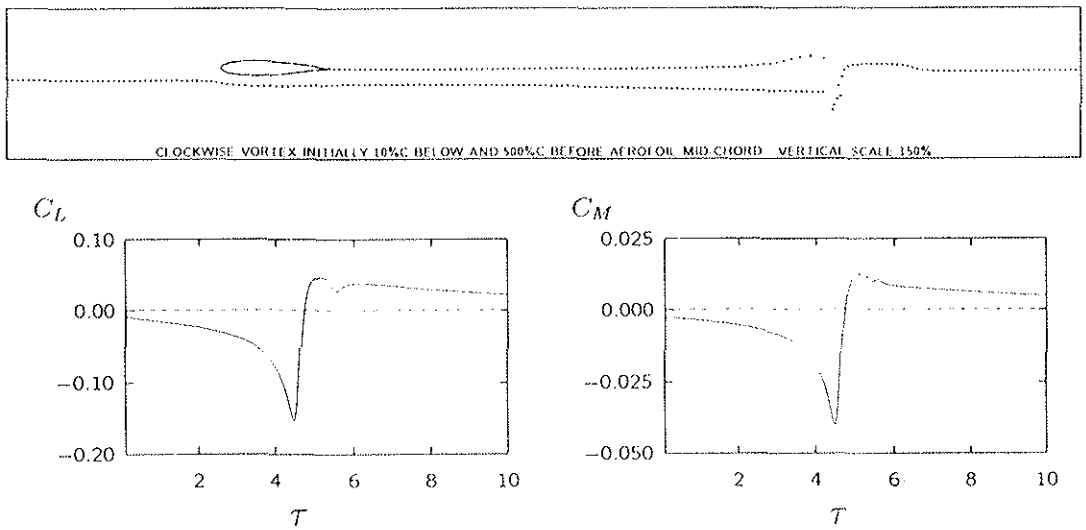

Figure 11: Vortex trajectory and C_L and C_M fluctuation during the interaction of a free vortex with a NACA0012 section flying at zero incidence relative to the undisturbed flow. The vortex passes the aerofoil leading edge at $\tau \approx 4.5$. ($\Gamma = 0.1$)

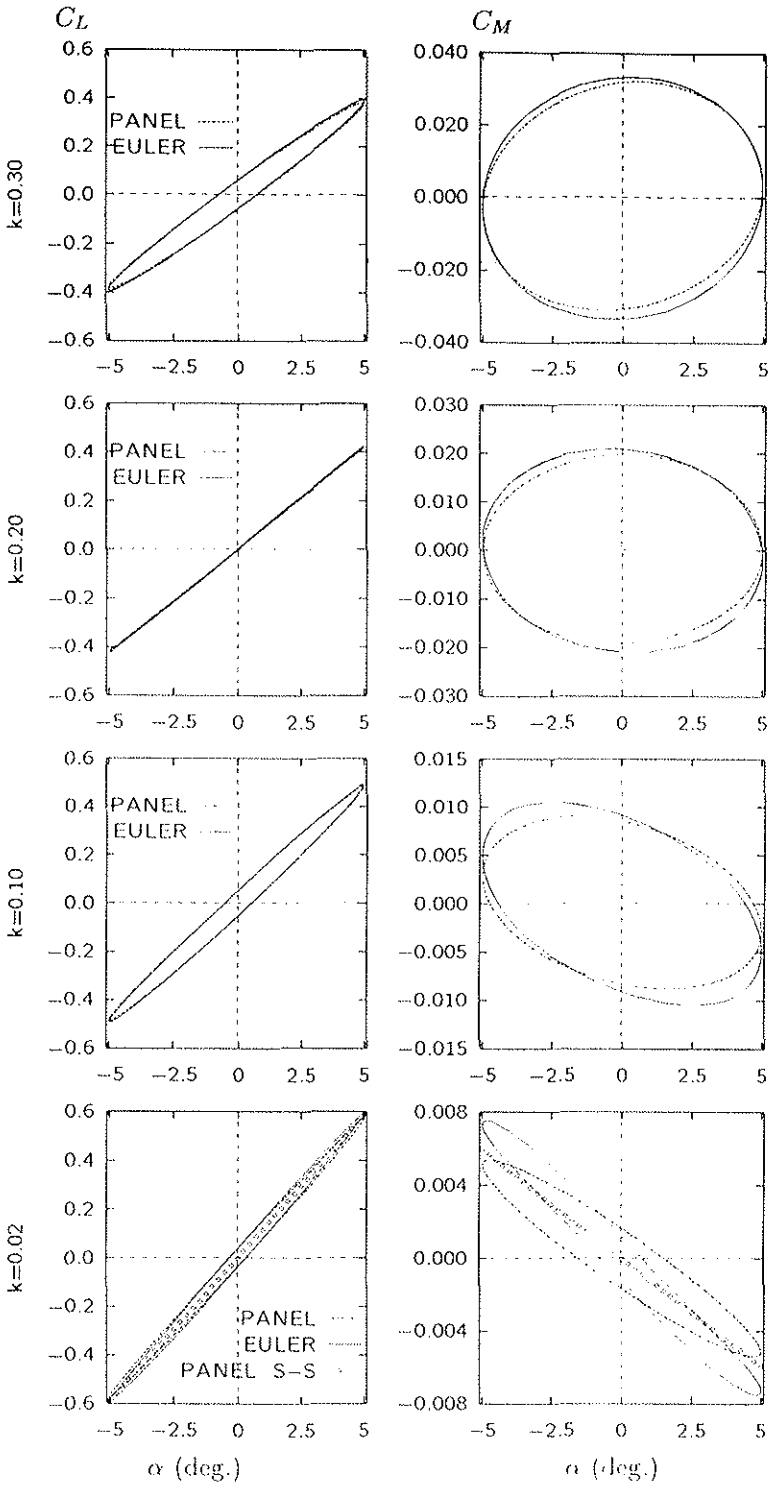

Figure 12: Comparison with EULER method results of Gaitonde[3] for the NACA0012 section in $\alpha = \sin 2k\tau$ pitching motion at zero mean incidence.

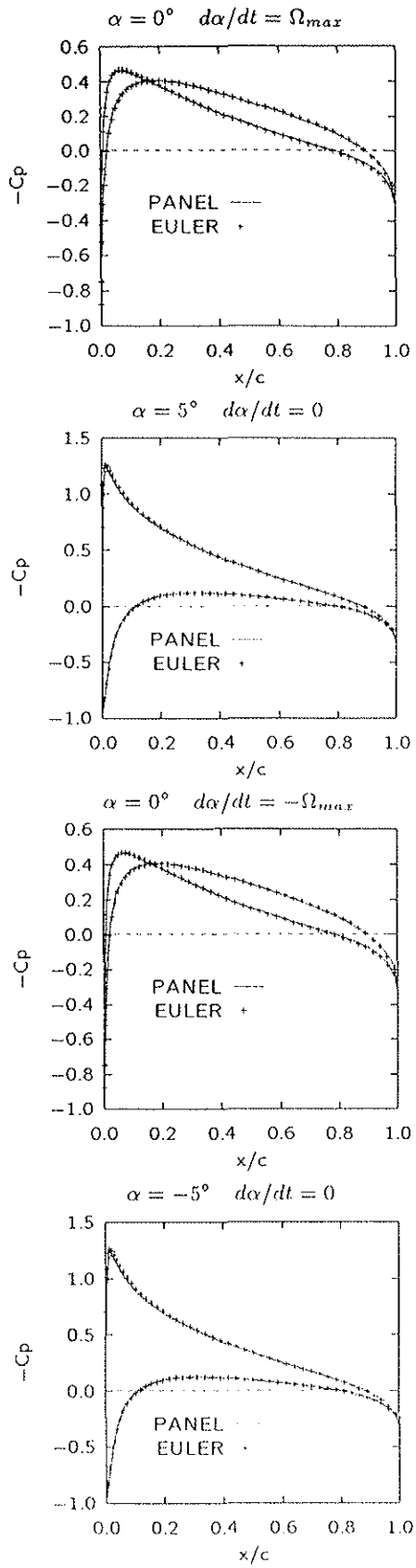

Figure 13: Comparison of pressure distributions at the quarter-phase positions of the NACA0012 section in pitch $\alpha = \alpha_o \sin 2k\tau$ for $k = 0.3$.

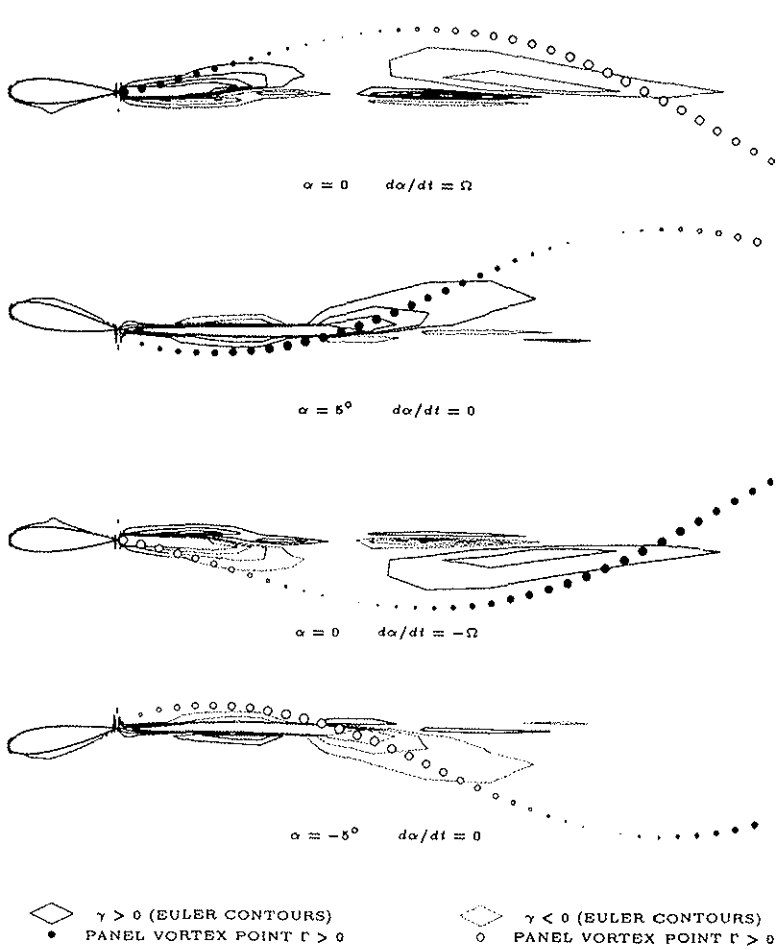

Figure 14: Euler-method vorticity contours with panel method wake geometry (wake strength indicated by point size) for the quarter-phase positions of the pitching motion (The vertical scale is exaggerated by ×2.)

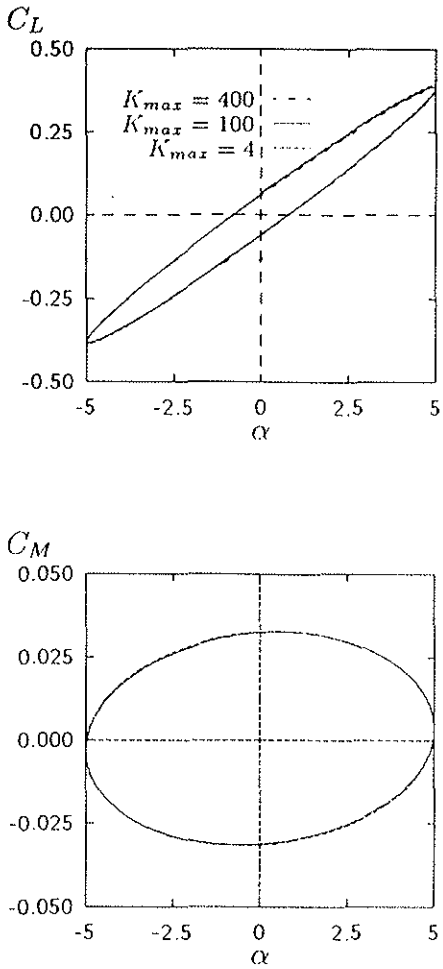

Figure 15. K_{max} sensitivity comparisons for NACA0012 in $\alpha = \sin 2k\tau$ motion at $k = 0.300$ with $n_{pc} = 400$.

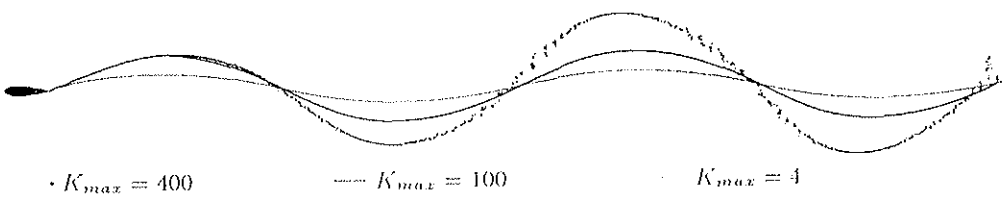

Figure 16: K_{max} sensitivity comparison of wake shapes for the NACA0012 after three cycles of $\alpha = \sin \omega t$ motion at $k = 0.300$ with $n_{pc} = 400$.